

Geophysical Research Letters®



RESEARCH LETTER

10.1029/2025GL117801

Key Points:

- We present the first quantitative evidence of the turbulence dissipation enhancement across the shock transition
- Turbulence energy dissipation rate is enhanced by 3 orders of magnitudes on average after shock transition
- Energy dissipation rates are higher under quasi-perpendicular shock conditions than under quasi-parallel ones

Supporting Information:

Supporting Information may be found in the online version of this article.

Correspondence to:

H. Li and W. Jiang,
hli@nssc.ac.cn;
jiangwence@swl.ac.cn

Citation:

Jiang, W., Li, H., Andrés, N., Hadid, L., Verscharen, D., & Wang, C. (2025). Significant amplification of turbulent energy dissipation through the shock transition at Mars. *Geophysical Research Letters*, 52, e2025GL117801. <https://doi.org/10.1029/2025GL117801>

Received 26 JUN 2025

Accepted 21 OCT 2025

Author Contributions:

Conceptualization: Wence Jiang, Hui Li, Daniel Verscharen, Chi Wang

Formal analysis: Wence Jiang, Hui Li, Nahuel Andrés, Lina Hadid, Daniel Verscharen, Chi Wang

Funding acquisition: Wence Jiang, Hui Li, Chi Wang

Methodology: Wence Jiang, Nahuel Andrés, Lina Hadid, Daniel Verscharen

Project administration: Wence Jiang, Hui Li, Chi Wang

Supervision: Hui Li, Chi Wang





Visualization: Wence Jiang

Writing – original draft: Wence Jiang

© 2025. The Author(s).

This is an open access article under the terms of the [Creative Commons Attribution-NonCommercial-NoDerivs License](#), which permits use and distribution in any medium, provided the original work is properly cited, the use is non-commercial and no modifications or adaptations are made.

Significant Amplification of Turbulent Energy Dissipation Through the Shock Transition at Mars

Wence Jiang¹ , Hui Li^{1,2} , Nahuel Andrés^{3,4}, Lina Hadid⁵, Daniel Verscharen⁶ , and Chi Wang^{1,2,7} 

¹State Key Laboratory of Solar Activity and Space Weather, National Space Science Center, Chinese Academy of Sciences, Beijing, China, ²School of Astronomy and Space Science, University of Chinese Academy of Sciences, Beijing, China, ³Facultad de Ciencias Exactas y Naturales, Departamento de Física, Universidad de Buenos Aires, Buenos Aires, Argentina, ⁴CONICET—Universidad de Buenos Aires, Instituto de Física Interdisciplinaria y Aplicada (INFIA), Buenos Aires, Argentina, ⁵Laboratoire de Physique des Plasmas, École Polytechnique, CNRS, Sorbonne University, Observatoire de Paris, University Paris–Sud, Palaiseau, France, ⁶Mullard Space Science Laboratory, University College London, Dorking, UK, ⁷College of Earth and Planetary Sciences, University of Chinese Academy of Sciences, Beijing, China

Abstract Turbulence is fundamental to energy transfer across scales in space and astrophysical plasmas. Bow shock interactions have long been hypothesized to significantly modify turbulence in planetary environments, yet the quantification of such effects and their parametric dependencies remain largely unaddressed. Using in situ long-term high-time resolution measurements from NASA's MAVEN mission, we report the first observational characterization of the evolution and parametric dependence of the turbulence energy cascade rate ε_c at magnetohydrodynamic (MHD) scales. Key findings reveal an averaged three-order-of-magnitude enhancement in ε_c when transitioning from the solar wind to the magnetosheath. Notably, downstream measurements of oblique and quasi-perpendicular shocks exhibit higher energy dissipation rates than those of quasi-parallel configurations. These results provide the first direct evidence linking shock obliquity to turbulence amplification, offering key insights into shock-mediated turbulence in similar but inaccessible systems.

Plain Language Summary Plasma turbulence plays a fundamental role in energy transport within space and planetary environments. However, the injection and dissipation of turbulent energy through the dramatic shock transition are not well understood. Mars, characterized by its compact magnetosheath and extended neutral exosphere, serves as an ideal natural laboratory for investigating solar wind turbulence around a non-magnetized planetary body. Using in situ measurements from NASA's MAVEN spacecraft, we reveal a distinct evolution pattern of turbulence across the Martian bow shock. Our findings reveal that turbulence energy dissipation is drastically amplified by three orders of magnitude post-shock, with a strong dependence on shock geometry. These results offer novel insights into the evolution of solar wind turbulence in compact, non-magnetized planetary environments, bridging a critical gap in our understanding of collisionless plasma dynamics.

1. Introduction

Turbulence within planetary magnetosheaths is a complex phenomenon characterized by nonlinear energy transfer and fluctuations arising from both upstream transport and local generation processes such as the shock interactions. In the pristine solar wind at 1 AU, magnetic field fluctuation power spectral densities (PSDs) typically exhibit three distinct power-law regimes separated by two spectral breaks. The small-scale break demarcates the transition from magnetohydrodynamic (MHD) scales to ion-kinetic scales (Bruno & Carbone, 2013; Sahraoui et al., 2020; Tu & Marsch, 1995; Verscharen et al., 2019). The large-scale break separates the characteristic MHD inertial range scaling ($f^{-5/3}$, where f is the frequency in the spacecraft frame) from a shallower f^{-1} scaling at larger scales. This spectral feature is also commonly observed in planetary magnetosheaths, such as those of Earth, Mars, Venus, and Saturn (Alexandrova, 2008; Czaykowska et al., 2001; Dwivedi et al., 2015; Hadid et al., 2015; Huang et al., 2017; Li et al., 2020; Ruhunusiri et al., 2017; Terres & Li, 2021). At ion scales, the transition range with steeper power law indices varying from -3 to -6.8 generally emerges between the inertial range and the $f^{-8/3}$ dissipation range (Duan et al., 2021; Huang et al., 2021; Sahraoui et al., 2020; Sioulas et al., 2023). However, within the Martian magnetosheath, magnetic field fluctuations frequently display a

Writing – review & editing:

Wence Jiang, Hui Li, Nahuel Andrés,
Lina Hadid, Daniel Verscharen, Chi Wang

plateau-like spectral feature, observed in approximately 57% of intervals, which exhibits a notable correlation with pickup ion (PUI) parameters (Jiang et al., 2023). Determining the nature of turbulent fluctuations is crucial and novel decomposition methods have been developed to determine the contribution of various MHD modes and coherent structures from the measured parameters (Lion et al., 2016; Zank et al., 2023). Previous studies in diverse space plasma environments indicate that the PSD encompasses a mixture of wave modes and coherent structures, including Alfvén waves, fast/slow-mode magnetosonic waves, filamentary Alfvén vortices, current sheets, and magnetic holes (Alexandrova, 2008; Huang et al., 2017; Jiang et al., 2022; Lion et al., 2016; Sahraoui et al., 2006; Vörös et al., 2008). These waves and structures span a wide range of scales and are essential for energy transfer and dissipation (Chasapis et al., 2018; Howes, 2016; Jiang et al., 2024; Osman et al., 2011).

The magnetosheath plasma undergoes significant transformations due to shock deceleration and compression, leading to pronounced variations in key parameters such as plasma- β (the ratio of thermal to magnetic pressure), temperature anisotropy, Alfvénic Mach number, turbulent Mach number, wave characteristics, and intermittency (Dimmock et al., 2014; Karimabadi et al., 2014; Li et al., 2020; Lucek et al., 2008; Sahraoui et al., 2006; Schwartz & Burgess, 1991; Soucek et al., 2015; Turc et al., 2023; Yordanova et al., 2008). Consequently, the properties of turbulent fluctuations in the magnetosheath are strongly modulated by the characteristics of the bow shock and the magnetopause (or, for weakly magnetized planets like Mars, the magnetic pile-up boundary (MPB)). Crucially, both the scale size and magnetic geometry of the bow shock, characterized by the angle Θ_{Bn} between the shock normal and the interplanetary magnetic field (IMF), modulate the spectral morphology and nature of downstream turbulent fluctuations (Alexandrova, 2008; Czakowska et al., 2001; Jiang et al., 2025; Li et al., 2020; Rakhmanova et al., 2018, 2020). During the MHD shock transition, previous studies have suggested that turbulent fluctuation amplitudes increase by one order of magnitude downstream quasi-perpendicular interplanetary shock (Pitňa et al., 2016, 2024; Zank et al., 2021). During a solar coronal mass ejection (CME) event, turbulence has also been examined before, during, and after the CME shock interactions and the highest energy cascade rate was observed in the CME sheath (Li et al., 2017; Marino & Sorriso-Valvo, 2023; Sorriso-Valvo et al., 2021). However, the evolution of turbulent energy transfer within the Martian magnetosheath and its dependence on specific shock parameters such as Θ_{Bn} remain largely unexplored, necessitating comprehensive statistical analyses to resolve these uncertainties.

Mars provides an exceptionally small spatial scale magnetosheath (approximately 5%–10% the size of Earth's magnetosheath,) which imposes fundamental constraints on turbulence development after shock interactions (Franco et al., 2024). Moreover, neutral particles that escape from the atmosphere undergo photo-ionization and charge exchange, producing PUIs in the solar wind rest frame with abundant free energy (Chamberlain, 1963; Cravens et al., 1987; Li et al., 2024; Rahmati et al., 2017; Romanelli et al., 2016). Injection of energy triggers the development of proton cyclotron waves (PCWs) and other modes within the Martian magnetosheath (Brain, 2002; Cowee et al., 2007, 2008; Cowee & Gary, 2012; Delva et al., 2015; Harada et al., 2019; Romanelli et al., 2013). This localized energy injection complicates our understanding of cross-scale energy transfer in the Martian magnetosheath. Enhanced turbulence energy cascade rates have been observed in the presence of PCWs or mirror modes both upstream and downstream of bow shocks in the solar system (Andrés et al., 2020; Hadid et al., 2018; Romanelli et al., 2022). A one-dimensional hybrid simulation suggests that wave energy in the form of PCWs gradually transfers inversely to larger wavelengths over time, particularly under conditions of strong injection (Cowee et al., 2008). The coupling between PUI instabilities and turbulence in Mars' compact magnetosheath—particularly its effects on spectral scaling and energy cascade, poses major challenges for modeling planetary plasma environments.

This study reports the first observational characterization of the turbulent energy cascade across the Martian shock transition, employing exact relations for fully developed compressible turbulence (Andrés & Sahraoui, 2017). Using unprecedented high-resolution measurements from NASA's MAVEN mission, we are able to quantify the turbulent energy cascade dependence on the bow shock geometry and the spatial evolution. Our results demonstrate significant spatial dependence of the turbulence energy cascade, characterized by the most enhanced cascade rates in the nose region of the magnetosheath. Furthermore, we establish functional dependencies of turbulent energy cascade rates on the shock normal angle (Θ_{Bn}) and the turbulent Mach number.

2. Data Set and Methods

2.1. Data Set

We use data from the Solar Wind Ion Analyzer (SWIA) (Halekas et al., 2015), the Suprathermal and Thermal Ion Composition (STATIC) analyzer (McFadden et al., 2015), and the Magnetometer (MAG) (Connerney et al., 2015) onboard MAVEN (Jakosky et al., 2015). The data set comprises a total of 11,098 magnetosheath intervals and 6,247 solar wind intervals from the years 2015 through 2019 (Jiang et al., 2023).

In order to make accurate estimations of the upstream solar wind and the interplanetary magnetic field at Mars, we assume that the state of the upstream solar wind detected by the MAVEN satellite remains approximately constant within a single orbit period (4.5 hr) and only use the upstream parameters within a single orbit period for each magnetosheath event. First, we eliminate interference caused by the upstream foreshock. Based on parametric criteria for the unperturbed pristine solar wind used in previous studies (Halekas et al., 2017), we identify the pristine solar wind by its velocity V_i , ion temperature T_i , normalized root-mean-square magnetic field perturbation σ_B/B_{sw} , and satellite orbit altitude L . We categorize intervals as pristine solar wind when simultaneously $V_i > 200$ km/s, $\sqrt{T_i}/V_i < 0.012$, $\sigma_B/B_{sw} < 0.15$, and $L > 500$ km, where $\sigma_B = \sqrt{\sum_{i=1}^3 \delta^2 B_i}$ is the root-mean-square value of the magnetic-field perturbation components.

We estimate the bow shock geometry based on the interplanetary magnetic field data in the upstream pristine solar wind and empirical conic and three-dimensional fitting models for the Martian bow shock (see more details in Supporting Information S1) (Gruesbeck et al., 2018; Trotignon et al., 2006). To determine the tangential point, we project the satellite position along the radial direction to the Mars center onto the bow shock surface (Li et al., 2020). Then, we calculate Θ_{Bn} as the angle between the bow shock normal direction and the interplanetary magnetic field at the projected point. For our statistical analysis, we calculate Θ_{Bn} for each single MAVEN orbit using the corresponding pristine solar-wind parameters.

2.2. Estimation of the Turbulence Energy Cascade Rates

Previous studies based their analysis of the energy cascade rate in incompressible MHD turbulence using the so-called Politano and Pouquet relation (Politano & Pouquet, 1998). Recent studies extend this framework to isothermal compressible MHD turbulence and successfully apply it to satellite observations and theoretical simulations for estimating turbulence energy cascade rates (Andrés et al., 2019, 2023; Andrés & Sahraoui, 2017; Brodiano et al., 2023; Hadid et al., 2018; Simon & Sahraoui, 2022).

For adiabatic compressible MHD equations, the compressible turbulent energy cascade rate (ϵ_c) satisfies (Andrés & Sahraoui, 2017)

$$-2\epsilon_c = \frac{1}{2} \nabla_l \cdot \mathbf{F}_C + S_C + S_H + M_\beta, \quad (1)$$

where \mathbf{F}_C is a flux term proportional to the perturbation two-point increments, S_C is a source term proportional to the divergence of the magnetic field and velocity field, S_H is a combined term of flux and source terms, and M_β is a mixed term related to the plasma- β . Assuming statistically isotropic fluctuations and neglecting all non-flux terms (Andrés et al., 2019), according to Taylor's hypothesis ($l = \mathbf{V}\tau$) (Taylor, 1937), we obtain

$$-\frac{4}{3}\epsilon_c l = F_{1C} + F_{2C}, \quad (2)$$

where the flux terms F_{1C} and F_{2C} can be expressed in terms of density ρ , velocity \mathbf{u} , and Alfvén velocity \mathbf{u}_A structure functions as

$$F_{1C} + F_{2C} = (\mathbf{F}_{1C} + \mathbf{F}_{2C}) \cdot \hat{\mathbf{V}}, \quad (3)$$

$$\mathbf{F}_{1C} = \langle [\delta(\rho\mathbf{u}) \cdot \delta\mathbf{u} + \delta(\rho\mathbf{u}_A) \cdot \delta\mathbf{u}_A] \delta\mathbf{u} - [\delta(\rho\mathbf{u}) \cdot \delta\mathbf{u}_A + \delta\mathbf{u} \cdot \delta(\rho\mathbf{u}_A)] \delta\mathbf{u}_A \rangle, \quad (4)$$

and

$$\mathbf{F}_{2C} = 2\langle \delta\rho \delta e \delta \mathbf{u} \rangle, \quad (5)$$

where $e = c_s^2 \ln(\rho/\rho_0)$ signifies the adiabatic closure (Andrés & Sahraoui, 2017). When the density perturbation is zero (i.e., the plasma is incompressible), ϵ_c in Equation 2 degenerates to the incompressible MHD turbulence energy cascade rate (Politano & Pouquet, 1998).

3. Results

3.1. Significant Amplification of Turbulent Energy Dissipation at Bow Shock

Figure 1 illustrates results from three distinct segments capturing turbulence characteristics in the upstream solar wind, quasi-parallel magnetosheath, and quasi-perpendicular magnetosheath at Mars, as observed by the MAVEN spacecraft on 22 November 2018, 02 December 2015, and 13 June 2016, respectively. The top four panels display the magnetic field components and magnitude, ion number density (n_i), ion velocity components, ion temperature and the β^* parameter, respectively. Here, $\beta^* = 2\mu_0(nk_B T_i + P_d)/|B|^2$, where k_B is the Boltzmann constant, T_i is the ion temperature, and $P_d = nm_p v_{sw}^2/2$ is the dynamic pressure. The fifth panel shows the ion differential energy flux spectrogram. All these measurements are acquired from the Solar Wind Ion Analyzer (Halekas et al., 2015) and the Magnetometer (Connerney et al., 2015) instruments onboard the MAVEN spacecraft (Jakosky et al., 2015). The magnetic field and ion velocity are depicted in the Mars Solar Orbital (MSO) coordinate system. The MPB serves as the inner boundary of the magnetosheath and is defined as the location where $\beta^* = 1$, indicating a balance between plasma (thermal and dynamic) pressure and magnetic pressure (Matsunaga et al., 2017). Panels f1 through f3 present the incompressible (PP98) and compressible (AS17) dissipation cascade rates as a function of the inverse time lag τ corresponding to the three segments highlighted by green, red, and blue shaded areas in the top five panels. Panels g1 through g3 show the spacecraft trajectory during the pristine solar wind (from UT 2018-11-22 02:30:00 to 03:30:00), quasi-parallel magnetosheath (from UT 2015-12-02 05:50:00 to 07:32:56), and quasi-perpendicular magnetosheath (from UT 2016-06-13 16:36:00 to 16:58:45) intervals, respectively.

We observe distinct characteristics in the plasma fluctuations of the solar wind and of the magnetosheath. Following interactions with the bow shock, notable ion heating occurs in the magnetosheath, accompanied by enhancements in magnetic-field strength, ion number density, and velocity fluctuations. To determine the geometries of the bow shock, we assume stationary solar wind conditions and utilize thresholds to estimate the average IMF in the corresponding pristine solar wind intervals for each magnetosheath segment (Halekas et al., 2017). Subsequently, we radially project the average spacecraft position onto the bow shock surface defined by the conic model (Trotignon et al., 2006) and calculate the angle Θ_{Bn} at the projection point. For the quasi-perpendicular (quasi-parallel) magnetosheath, we find $\Theta_{Bn} = 87^\circ$ ($\Theta_{Bn} = 9.8^\circ$), as illustrated by Figure 1g1.

Applying the exact relation for fully developed turbulence, we estimated the incompressible (PP98) and compressible (AS17) MHD energy cascade rates (Andrés & Sahraoui, 2017; Politano & Pouquet, 1998) (see Section 2.2). Figure 1 shows the estimation of energy cascade rate both for (f1) the pristine solar wind (f2) quasi-parallel magnetosheath, and (f3) quasi-perpendicular magnetosheath, respectively. The gray dashed vertical lines indicate the minimum reliable scale τ_0 (i.e., half of the event duration), above which estimations are unreliable. The magnetic-field spectra in the Martian magnetosheath often present plateau-like triple power-laws (Jiang et al., 2023). This observation suggests that the turbulence in the magnetosheath is not fully developed due to ongoing injection of energy, especially at ion scales. Therefore, we consider the energy cascade rates only for the large-scale inertial range exhibiting a linear scaling in the magnetic-field spectra. We estimate the energy cascade rates by averaging the absolute value of ϵ over $313 s < \tau < T/2$, where 313 s corresponds approximately to the scale where the inertial range ends, as suggested by our statistics of the spectral break frequencies (see more details in Supporting Information S1), and T is the total duration of each given interval. For consistency, we calculate all the average energy cascade rates in our following statistical analysis using the same criteria.

We observe significantly higher magnetosheath cascade rates when we compared to those in the pristine solar wind. Specifically, these results do not show a dependence with the bow shock geometry. However, when we compared the quasi-perpendicular interval with respect to the quasi-parallel interval, we observe notably higher average cascade rates in the quasi-perpendicular event. In particular, the incompressible and compressible quasi-

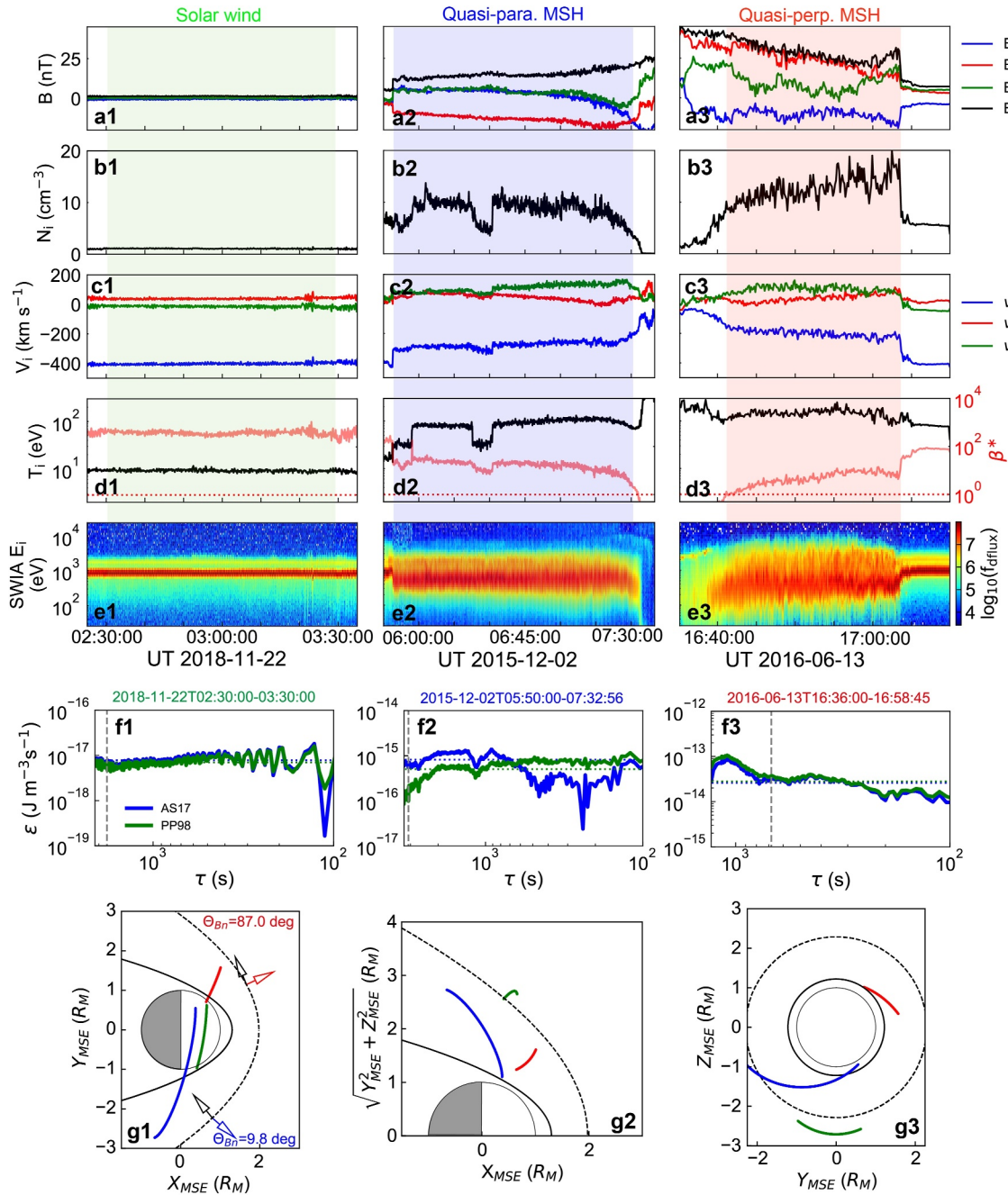


Figure 1. MAVEN observations in the solar wind, quasi-parallel, and quasi-perpendicular magnetosheath regions at Mars. The panels display, from top to bottom, (a) the magnetic field components and magnitude, (b) the ion number density, (c) the ion bulk velocity components, (d) the ion temperature and β^* parameter, (e) the ion differential energy flux spectrogram as a function of time, respectively. The red (blue) shaded areas indicate the magnetosheath regions behind the quasi-perpendicular (quasi-parallel) bow shock. The green shaded areas mark pristine solar wind intervals. Panels (f) show the energy cascade rates as a function of time lag, the horizontal blue and green dotted lines denote the average cascade rates. Panels (g) display the spacecraft's trajectory in the Mars Solar Electric (X, Y) plane, ($X, \sqrt{Y^2 + Z^2}$) plane, and (Y, Z) plane, respectively. The colored lines in panels (g) depict the spacecraft trajectories during the quasi-perpendicular (red), quasi-parallel (blue) magnetosheath and pristine solar wind (green) intervals. The black dashed and solid lines represent the positions of the bow shock and the magnetic pile-up boundary.

perpendicular magnetosheath cascade rates are $3.35 \times 10^{-14} \text{ J m}^{-3} \text{ s}^{-1}$ (PP98) and $3.11 \times 10^{-14} \text{ J m}^{-3} \text{ s}^{-1}$ (AS17), respectively, while the quasi-parallel magnetosheath cascade rates are $4.84 \times 10^{-16} \text{ J m}^{-3} \text{ s}^{-1}$ (PP98) and $8.59 \times 10^{-16} \text{ J m}^{-3} \text{ s}^{-1}$ (AS17), respectively. In comparison, the solar wind turbulence energy cascade rates are $6.78 \times 10^{-18} \text{ J m}^{-3} \text{ s}^{-1}$ (PP98) and $7.59 \times 10^{-18} \text{ J m}^{-3} \text{ s}^{-1}$ (AS17). We find these values in the solar wind are

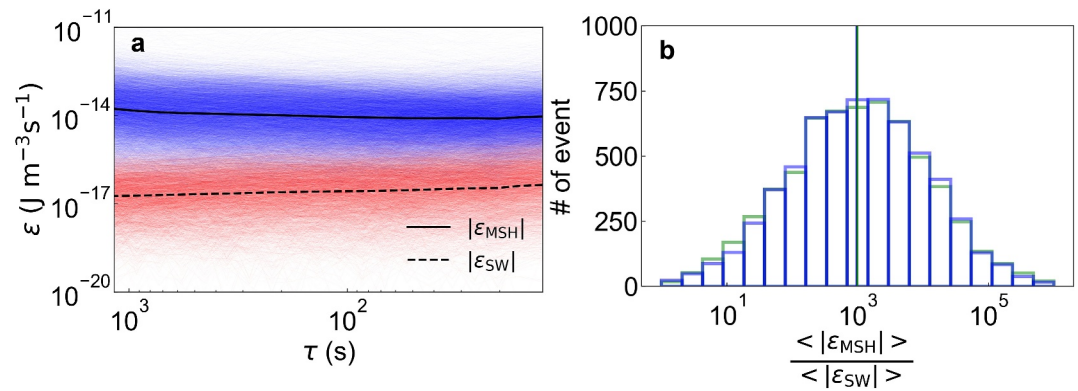


Figure 2. (a) Superposition of the compressible turbulent energy cascade rate as a function of time lag for all events. Black solid and dashed lines indicate the average cascade rates. (b) The distribution of the average ratios of compressible (blue) and incompressible (green) turbulent energy cascade rates, while the green and blue vertical lines denote its average.

similar to previous results reported at Mars (Andrés et al., 2020; Romanelli et al., 2022), but about one order of magnitude smaller than those reported in previous studies at 1 AU (Hadid et al., 2017). In particular, the turbulent energy cascade rates in the Martian magnetosheath are significantly smaller than those in Earth's magnetosheath (Andrés et al., 2020; Hadid et al., 2018). We observe an increase of three orders of magnitude in the turbulent energy cascade rates across the bow shock, with average ratios ranging from 3,385 to 4,022 for the quasi-perpendicular region and 72–106 for the quasi-parallel region. In addition, the quasi-parallel magnetosheath event exhibits an enhanced increase in the cascade rate attributed to significant density perturbations, as depicted in Figure 1f2. The quasi-perpendicular event also shows a significant increase in the density perturbations.

Figure 2 summarizes our statistical analysis of the turbulent energy cascade rate in the solar wind and the magnetosheath. Figure 2a shows the compressible MHD turbulent cascade rates estimated for a total of 11,098 magnetosheath intervals and 6,247 solar wind intervals spanning from 2015 to 2019 (Jiang et al., 2023). Figure 2b displays the histogram of ratios of turbulent energy cascade rates in the magnetosheath and in the solar wind. The colored bins in blue (green) represent results for compressible (incompressible) turbulent cascade rates. The average compressible turbulent cascade rate is $1.99 \times 10^{-17} \text{ J m}^{-3} \text{ s}^{-1}$ in the solar wind and $2.27 \times 10^{-14} \text{ J m}^{-3} \text{ s}^{-1}$ in the magnetosheath. The average ratio between the compressible turbulence energy cascade rates in the magnetosheath and the solar wind is very close to that for incompressible cascade rates (1,198.44 vs. 1,260.11). In addition, the compressible (incompressible) turbulent energy cascade rates show no significant variation throughout the Martian seasons as a function of the solar longitude of Mars or the level of EUV irradiance, which is directly related to the density of PUIs (see Figure S3 in Supporting Information S1).

3.2. Spatial and Parametric Dependence of the Turbulence Evolution

Figure 3a shows a color map of the average compressible cascade rates in the $(X, \text{sign}(Y) \cdot \sqrt{Y^2 + Z^2})$ MSE plane. Data points are organized into a grid of 40×40 evenly spaced bins in the ranges $3 > X > -1.7$ and $3 > \text{sign}(Y) \cdot \sqrt{Y^2 + Z^2} > -3$. The color represents average compressible turbulent energy cascade rate in each bin. Figure 3b shows average compressible cascade rate in the magnetosheath under quasi-parallel (red) and quasi-perpendicular (blue) shock conditions as a function of the distance from the center of Mars. Figures 3c–3e displays the compressible (AS17) and incompressible (PP98) cascade rates in the solar wind and magnetosheath, along with the ratio of turbulence energy cascade rates as functions of the angle Θ_{Bn} . The data are binned into an evenly spaced grid with $0 < \Theta_{\text{Bn}} < 90^\circ$.

Our statistical analysis confirms a distinct transition in the incompressible and compressible cascade rates when MAVEN crosses the bow shock. More specifically, we observe a significant enhancement in the cascade rate downstream of the shock, especially in the shock nose region. Radially, the average cascade rates increase approximately by a factor of 1,000 when crossing from the solar wind into the magnetosheath. Figures 3c and 3d reveals that compressible cascade rates generally exceed incompressible cascade rates regardless of shock geometry (i.e., independent of Θ_{Bn}). In the upstream solar wind, the turbulence energy cascade rates show minimal

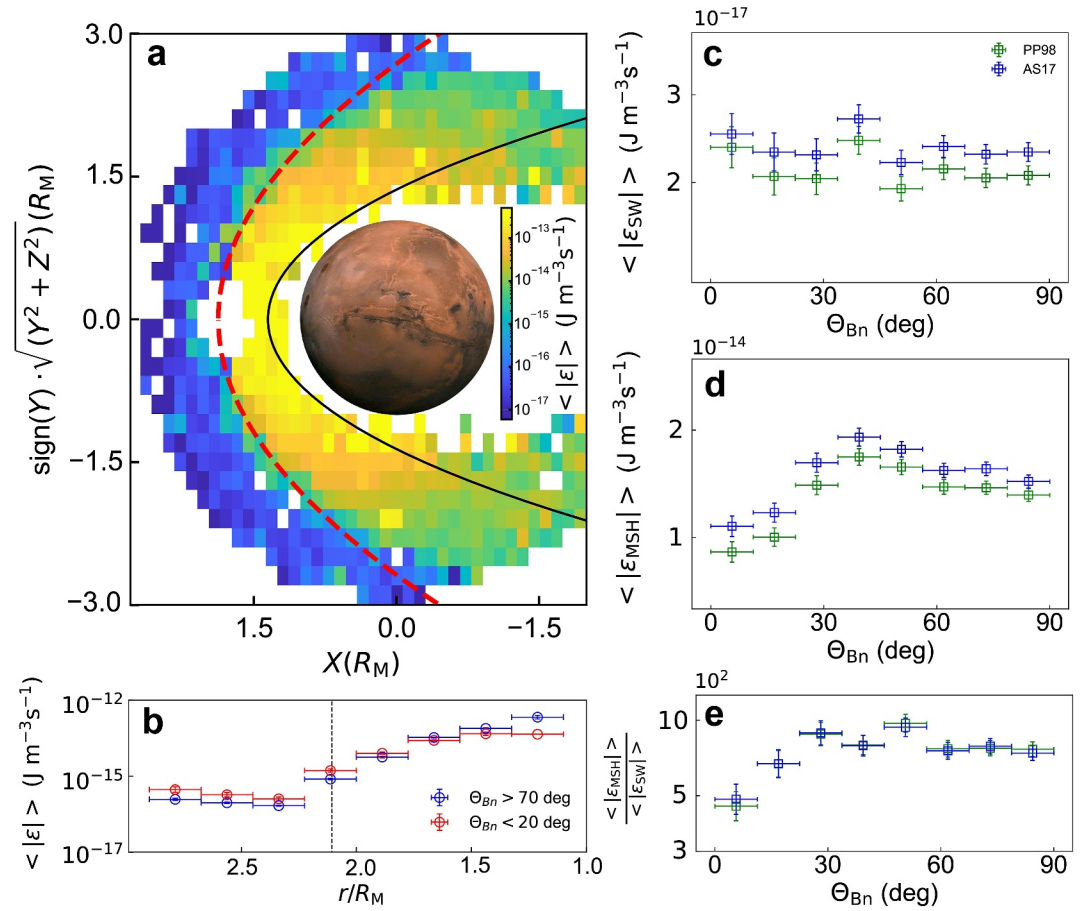


Figure 3. (a) Distribution map of compressible turbulence energy cascade rates (AS17) in the $(X, \text{sign}(Y) \cdot \sqrt{Y^2 + Z^2})$ plane in MSE coordinates. The red dashed and black solid lines denote the nominal positions of the bow shock and the magnetic pile-up boundary. (b) Compressible turbulence energy cascade rates (AS17) plotted against distance from the center of Mars. The black vertical line indicates the nominal position of the bow shock. Compressible (blue) and incompressible (green) turbulence energy cascade rates as a function of the bow shock normal angle (c) in the solar wind and (d) in the magnetosheath. (e) Ratios of compressible (blue) and incompressible (green) turbulence energy cascade rates from the solar wind to the magnetosheath based on the bow shock normal angle.

dependence on Θ_{Bn} and are slightly greater for quasi-parallel bow shock conditions than for quasi-perpendicular conditions. However, in the magnetosheath, turbulence energy cascade rates exhibit a clear dependence on Θ_{Bn} with a peak value around $\Theta_{Bn} \approx 45^\circ$. Overall, quasi-perpendicular ($\Theta_{Bn} > 45^\circ$) magnetosheath turbulence displays greater cascade rates compared to quasi-parallel ($\Theta_{Bn} < 45^\circ$) magnetosheath turbulence. Figure 3e shows that the enhancement ratio when crossing the bow shock increases with Θ_{Bn} from approximately 400 ($\Theta_{Bn} \approx 10^\circ$) to nearly 1,000 ($\Theta_{Bn} > 30^\circ$).

To evidence different levels of density and velocity fluctuations downstream of different shock geometries, we show the local turbulent Mach number $M_{\text{turb}} = \sqrt{(\delta v)^2 / c_s^2}$ (c_s is the sound speed) and the root-mean-square ion density perturbation δn_{RMS} as functions of the shock normal angle in Figure 4a. In Figure 4b, we also find a positive correlation between compressible energy cascade rates in the solar wind and magnetosheath with the turbulent Mach number M_{turb} , showing correlation coefficients ranging from 0.52 to 0.57. Note that we limit our interpretation of the effect of compressibility to the results of compressible energy cascade rates. Using a linear fitting approach, we find a shallower slope for the energy cascade rate in the Martian magnetosheath (1.93) compared to those previously reported in Earth's magnetosheath (3.8 for Alfvénic events or 4.1 for magnetosonic events, see details in Hadid et al., 2018). The average M_{turb} in the magnetosheath initially increases and then declines with increasing Θ_{Bn} , reaching its peak at $\Theta_{Bn} \approx 20^\circ$. Unlike M_{turb} , the density fluctuation level δn_{RMS} shows a different dependence on Θ_{Bn} . Since M_{turb} represents a measure of the fluctuating velocity, this result

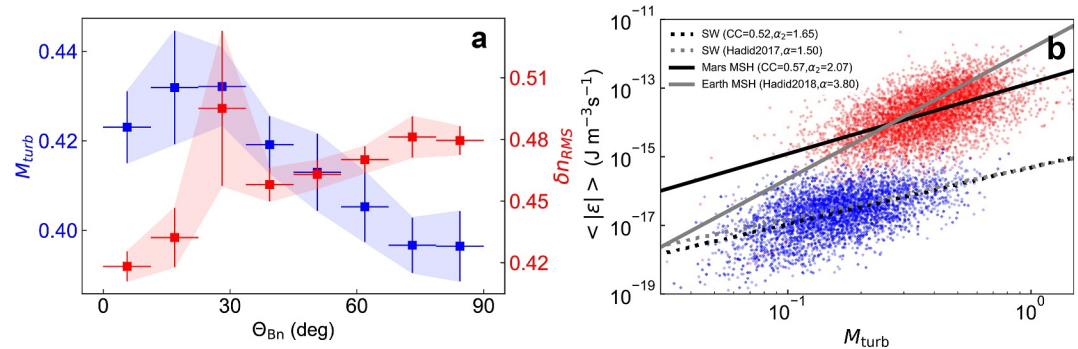


Figure 4. (a) The magnetosheath M_{turb} and root-mean-square ion density perturbation δn_{RMS} as functions of the shock normal angle. The error bars represent standard error of the mean value (vertical) and the extent of the bin (horizontal). (b) Solar wind and magnetosheath turbulence energy cascade rates as a function of the local turbulent Mach number M_{turb} . Dotted and solid lines represent linear scaling laws from fitting and previous studies at 1 AU (Hadid et al., 2017, 2018).

indicates that plasma compressibility could somehow enhance and compensate for the turbulence energy cascade rates in the Martian magnetosheath, leading to a more significant enhancement downstream of quasi-perpendicular shocks. Moreover, the shallow slope for the cascade rates in the Martian magnetosheath suggests that the subsonic ($M_{\text{turb}} < 1$) turbulence is somehow less “compressible” in a way different from Earth’s highly compressible magnetosheath and the nearly incompressible solar wind turbulence. However, there is no theoretical prediction that explains the different scalings between M_{turb} and the compressible turbulence energy cascade rates reported by recent in situ observations. Combined with our previous findings on the dependence of the average cascade rates on Θ_{Bn} , this result suggests that both M_{turb} and δn_{RMS} are affecting the energy cascade rates in compressible turbulence.

4. Discussion and Conclusion

We present a comprehensive analysis of compressible turbulence energy cascade rates upstream and downstream of the bow shock at Mars, using high-time-resolution magnetic field and ion data from the MAVEN mission. To the best of our knowledge, our observational results are the first presentation of a statistical map of turbulent cascade in the Martian environment, revealing a remarkable spatial evolution and location dependence.

Interactions at the bow shock lead to a significant increase in the turbulent energy cascade rate. More specifically, transitioning from the upstream solar wind to the downstream magnetosheath, compressible turbulent energy cascades experience a substantial enhancement by two or three orders of magnitude. In the upstream solar wind, the energy cascade rates are evenly distributed in space. In the magnetosheath, however, we observe a significant increase in the cascade rates downstream of the bow shock nose, gradually decreasing as the plasma flows towards the flank regions. The cascade rates increase as the spacecraft’s distance decreases from the center of Mars, increasing by more than a factor of 10 from the bow shock vicinity to the magnetic pile-up boundary. Moreover, our further analysis also suggests that the turbulent energy cascade rates decrease as the magnetic-field spectral index increases. This is in part consistent with a previous study (Andrés et al., 2020), suggesting that local energy injections from waves generated by PUIs in the magnetosheath may suppress the turbulent cascade. However, there is no significant dependence of the turbulent energy cascade rates on the Martian season or the level of solar extreme ultraviolet irradiance, which is related to PUI processes.

By categorizing the geometries of the bow shock, our results further reveal that the increases in the turbulent energy cascade rates are significantly greater in the quasi-perpendicular region compared to the quasi-parallel region. While the solar wind cascade rates remain approximately constant, independently of the shock normal angle (Θ_{Bn}), the magnetosheath turbulence energy cascade rates vary, with greater values observed under oblique and quasi-perpendicular shock conditions. In both the solar wind and magnetosheath plasma, compressible cascade rates generally exceed incompressible turbulence energy cascade rates, indicating that density fluctuations enhance energy cascade rates as indicated by previous results (Andrés et al., 2019, 2021; Ferrand et al., 2022; Hadid et al., 2017, 2018). We observe a positive correlation between turbulence energy cascade rates

in both the solar wind and magnetosheath with the turbulent Mach number M_{turb} , partially consistent with previous result in Earth's magnetosheath (Hadid et al., 2018). Although we find a remarkable agreement of the linear scaling laws in the solar wind turbulence at 1 AU and at Mars, the scaling law in the Martian magnetosheath is quite different from Earth's magnetosheath, requiring further theoretical investigation to explain different scaling laws. Our analysis also suggests that the enhancement of turbulence energy cascade rates in the Martian magnetosheath is influenced by both the levels of density and velocity perturbations. Downstream of quasi-perpendicular shocks, a higher level of plasma compressibility leads to generally higher energy cascade rates compared to quasi-parallel shocks.

Our observational findings offer new insights into the impact of bow-shock interactions on magnetosheath turbulence at Mars. Quantitative analysis shows that the magnetosheath turbulence energy cascade rate is significantly amplified by three orders of magnitude due to the shock compression. Turbulence in the quasi-perpendicular magnetosheath presents a more compressible state compared to the quasi-parallel magnetosheath, hence greater energy cascade rates. However, several challenges persist in understanding the key parameters governing the nonlinear cascade and dissipation of energy. For instance, the exact impact of local instabilities injected by either shock interactions or PUIs in the Martian environment on turbulence energy cascade remains unclear (Andrés et al., 2020; Jiang et al., 2023; Li et al., 2024; Romanelli et al., 2022; Ruhunusiri et al., 2017). We emphasize that our calculations of energy cascade rates cover only the large scales and exclude scales close to the spectral plateau or ion scales. We acknowledge that turbulence may not be fully developed in the Martian magnetosheath, meaning that we cannot strictly guarantee that forcing scales are at the largest scales, dissipation scales at the smallest scale, and a clean inertial range in between. We also cannot be certain that the plasma is homogeneous, which is a strong assumption in the derivation of the third-order laws. Still, we use the third-order laws because they provide accessible information from time series (Andrés et al., 2023; Bandyopadhyay et al., 2021; Huang et al., 2017; Li et al., 2020). The complex interplay between the nonlinear evolution of waves and background turbulent fluctuations necessitates further investigation. Future multi-point missions, such as the European Space Agency's M-MATISSE science mission candidate (Sanchez-Cano et al., 2022), may offer new insight by simultaneously monitoring upstream and downstream conditions around the Martian bow shock.

Conflict of Interest

The authors declare no conflicts of interest relevant to this study.

Data Availability Statement

All data used in the paper and the Supporting Information S1 are publicly available through the Planetary Data System: <https://pds-ppi.igpp.ucla.edu/mission/MAVEN/MAVEN/MAG> for MAG (Connerney, 2024) and <https://pds-ppi.igpp.ucla.edu/mission/MAVEN/MAVEN/SWIA> for SWIA (Halekas, 2024). Data analysis was performed using the Space Physics Environment Data Analysis System (SPEDAS) (Angelopoulos et al., 2024).

Acknowledgments

The authors thank the entire MAVEN team for providing the data. This work is supported by the NNSFC Grants (Grant 42374198, 42188101, 42404177), project of Civil Aerospace "14th Five Year Plan" Preliminary Research in Space Science (D010302, D010202). W.J. is supported by NSSC Youth grant and the Specialized Research Fund for State Key Laboratories of China. H.L. is also supported by the China-Brazil Joint Laboratory for Space Weather (No. 119GJHZ2024027MI). D.V. is supported by STFC Consolidated Grant ST/W001004/1. N.A. acknowledges financial support from the following grants: PIP Grant 11220200101752 and Redes de Alto Impacto REMATE from Argentina.

References

- Alexandrova, O. (2008). Solar wind vs magnetosheath turbulence and Alfvén vortices. *Nonlinear Processes in Geophysics*, 15(1), 95–108. <https://doi.org/10.5194/npg-15-95-2008>
- Andrés, N., Bandyopadhyay, R., McComas, D., Szalay, J., Allegrini, F., Ebert, R., et al. (2023). Observation of turbulent magnetohydrodynamic cascade in the Jovian magnetosheath. *The Astrophysical Journal*, 945(1), 8. <https://doi.org/10.3847/1538-4357/acb7e0>
- Andrés, N., Romanelli, N., Hadid, L. Z., Sahraoui, F., DiBraccio, G., & Halekas, J. (2020). Solar wind turbulence around Mars: Relation between the energy cascade rate and the proton cyclotron waves activity. *The Astrophysical Journal*, 902(2), 134. <https://doi.org/10.3847/1538-4357/abb5a7>
- Andrés, N., & Sahraoui, F. (2017). Alternative derivation of exact law for compressible and isothermal magnetohydrodynamics turbulence. *Physical Review*, 96(5), 053205. <https://doi.org/10.1103/PhysRevE.96.053205>
- Andrés, N., Sahraoui, F., Galtier, S., Hadid, L. Z., Ferrand, R., & Huang, S. Y. (2019). Energy cascade rate measured in a collisionless space plasma with MMS data and compressible hall magnetohydrodynamic turbulence theory. *Physical Review Letters*, 123(24), 245101. <https://doi.org/10.1103/PhysRevLett.123.245101>
- Andrés, N., Sahraoui, F., Hadid, L. Z., Huang, S. Y., Romanelli, N., Galtier, S., et al. (2021). The evolution of compressible solar wind turbulence in the inner heliosphere: PSP, THEMIS and MAVEN observations. *ApJ*, 919(1), 19. <https://doi.org/10.3847/1538-4357/ac0af5>
- Angelopoulos, V., Cruce, P., Drozdov, A., Grimes, E. W., Hatzigeorgiu, N., King, D. A., et al. (2024). SPEDAS: Space physics environment data analysis system [Software]. *Astrophysics Source Code Library*. <https://ui.adsabs.harvard.edu/abs/2024ascl.soft05001A/abstract>
- Bandyopadhyay, R., McComas, D. J., Szalay, J. R., Allegrini, F., Bolton, S. J., Ebert, R. W., et al. (2021). Observation of Kolmogorov turbulence in the Jovian magnetosheath from JADE data. *Geophysical Research Letters*, 48(15), e2021GL095006. <https://doi.org/10.1029/2021GL095006>

- Brain, D. A., Bagenal, F., Acuña, M. H., Connerney, J. E. P., Crider, D. H., Mazelle, C., et al. (2002). Observations of low-frequency electromagnetic plasma waves upstream from the Martian shock. *Journal of Geophysical Research*, 107(A6), 1076. <https://doi.org/10.1029/2000JA000416>
- Brodiano, M., Dmitruk, P., & Andrés, N. (2023). A statistical study of the compressible energy cascade rate in solar wind turbulence: Parker solar probe observations. *Physics of Plasmas*, 30(3), 032903. <https://doi.org/10.1063/5.0109379>
- Bruno, R., & Carbone, V. (2013). The solar wind as a turbulence laboratory. *Living Reviews in Solar Physics*, 10. <https://doi.org/10.12942/lrsp-2013-2>
- Chamberlain, J. W. (1963). Planetary coronae and atmospheric evaporation. *Planetary and Space Science*, 11(8), 901–960. [https://doi.org/10.1016/0032-0633\(63\)90122-3](https://doi.org/10.1016/0032-0633(63)90122-3)
- Chasapis, A., Matthaeus, W. H., Parashar, T. N., Wan, M., Haggerty, C. C., Pollock, C. J., et al. (2018). In situ observation of intermittent dissipation at kinetic scales in the Earth's magnetosheath. *The Astrophysical Journal Letters*, 856(1), L19. <https://doi.org/10.3847/2041-8213/aaadf8>
- Connerney, J. E. P. (2024). NASA planetary data System [Dataset]. <https://doi.org/10.17189/1414249>
- Connerney, J. E. P., Espley, J., Lawton, P., Murphy, S., Odom, J., Oliverson, R., & Sheppard, D. (2015). The MAVEN magnetic field investigation. *Space Science Reviews*, 195(1–4), 257–291. <https://doi.org/10.1007/s11214-015-0169-4>
- Cowee, M. M., & Gary, S. P. (2012). Electromagnetic ion cyclotron wave generation by planetary pickup ions: One-dimensional hybrid simulations at sub-Alfvénic pickup velocities: Pickup ion waves in sub-Alfvénic regime. *Journal of Geophysical Research*, 117(A6), A06215. <https://doi.org/10.1029/2012JA017568>
- Cowee, M. M., Russell, C. T., & Strangeway, R. J. (2008). One-dimensional hybrid simulations of planetary ion pickup: Effects of variable plasma and pickup conditions: Simulations of ion pickup conditions. *Journal of Geophysical Research*, 113(A8), n/a–n/a. <https://doi.org/10.1029/2008JA013066>
- Cowee, M. M., Winske, D., Russell, C. T., & Strangeway, R. J. (2007). 1D hybrid simulations of planetary ion-pickup: Energy partition. *Geophysical Research Letters*, 34(2), L02113. <https://doi.org/10.1029/2006GL028285>
- Cravens, T. E., Kozyra, J. U., Nagy, A. F., Gombosi, T. I., & Kurtz, M. (1987). Electron impact ionization in the vicinity of comets. *Journal of Geophysical Research*, 92(A7), 7341–7353. <https://doi.org/10.1029/JA092iA07p07341>
- Czaykowska, A., Bauer, T. M., Treumann, R. A., & Baumjohann, W. (2001). Magnetic field fluctuations across the Earth's bow shock. *Annales Geophysicae*, 19(3), 275–287. <https://doi.org/10.5194/angeo-19-275-2001>
- Delva, M., Bertucci, C., Volwerk, M., Lundin, R., Mazelle, C., & Romanelli, N. (2015). Upstream proton cyclotron waves at Venus near solar maximum. *Journal of Geophysical Research: Space Physics*, 120(1), 344–354. <https://doi.org/10.1002/2014JA020318>
- Dimmock, A. P., Nykyri, K., & Pulkkinen, T. I. (2014). A statistical study of magnetic field fluctuations in the dayside magnetosheath and their dependence on upstream solar wind conditions. *Journal of Geophysical Research: Space Physics*, 119(8), 6231–6248. <https://doi.org/10.1002/2014JA020009>
- Duan, D., He, J., Bowen, T. A., Woodham, L. D., Wang, T., Chen, C. H. K., et al. (2021). Anisotropy of solar wind turbulence in the inner heliosphere at kinetic scales: PSP observations. *The Astrophysical Journal Letters*, 915(1), L8. <https://doi.org/10.3847/2041-8213/ac07ac>
- Dwivedi, N. K., Schmid, D., Narita, Y., Kovács, P., Vörös, Z., Delva, M., & Zhang, T. (2015). Statistical investigation on the power-law behavior of magnetic fluctuations in the Venusian magnetosheath. *Earth Planets and Space*, 67(1), 137. <https://doi.org/10.1186/s40623-015-0308-x>
- Ferrand, R., Sahraoui, F., Galtier, S., Andrés, N., Mininni, P., & Dmitruk, P. (2022). An in-depth numerical study of exact laws for compressible hall magnetohydrodynamic turbulence. *ApJ*, 927(2), 205. <https://doi.org/10.3847/1538-4357/ac517a>
- Franco, A. M. S., Echer, E., Fränz, M., & Bolzan, M. J. A. (2024). Intermittent plasma turbulence in the Martian plasma environment. *Reviews of Modern Plasma Physics*, 8(1), 3. <https://doi.org/10.1007/s41614-023-00141-4>
- Gruesbeck, J. R., Espley, J. R., Connerney, J. E. P., DiBraccio, G. A., Soobiah, Y. I., Brain, D., et al. (2018). The three-dimensional bow shock of Mars as observed by MAVEN. *Journal of Geophysical Research: Space Physics*, 123(6), 4542–4555. <https://doi.org/10.1029/2018JA025366>
- Hadid, L. Z., Sahraoui, F., & Galtier, S. (2017). Energy cascade rate in compressible fast and slow solar wind turbulence. *ApJ*, 838(1), 9. <https://doi.org/10.3847/1538-4357/aa603f>
- Hadid, L. Z., Sahraoui, F., Galtier, S., & Huang, S. Y. (2018). Compressible magnetohydrodynamic turbulence in the Earth's magnetosheath: Estimation of the energy Cascade rate using *in situ* spacecraft data. *Physical Review Letters*, 120(5), 055102. <https://doi.org/10.1103/PhysRevLett.120.055102>
- Hadid, L. Z., Sahraoui, F., Kiyani, K. H., Retinò, A., Modolo, R., Canu, P., et al. (2015). Nature of the MHD and kinetic scale turbulence in the magnetosheath of Saturn: Cassini observations. *The Astrophysical Journal*, 813(2), L29. <https://doi.org/10.1088/2041-8205/813/2/L29>
- Halekas, J. S. (2024). NASA planetary data system [Dataset]. <https://doi.org/10.17189/1414246>
- Halekas, J. S., Ruhunusiri, S., Harada, Y., Collinson, G., Mitchell, D. L., Mazelle, C., et al. (2017). Structure, dynamics, and seasonal variability of the Mars-solar wind interaction: MAVEN solar wind ion analyzer in-flight performance and science results. *Journal of Geophysical Research: Space Physics*, 122(1), 547–578. <https://doi.org/10.1002/2016JA023167>
- Halekas, J. S., Taylor, E. R., Dalton, G., Johnson, G., Curtis, D. W., McFadden, J. P., et al. (2015). The solar wind ion analyzer for MAVEN. *Space Science Reviews*, 195(1–4), 125–151. <https://doi.org/10.1007/s11214-013-0029-z>
- Harada, Y., Ruhunusiri, S., Halekas, J. S., Espley, J., DiBraccio, G. A., McFadden, J. P., et al. (2019). Locally generated ULF waves in the Martian magnetosphere: MAVEN observations. *Journal of Geophysical Research: Space Physics*, 124(11), 8707–8726. <https://doi.org/10.1029/2019JA027312>
- Howes, G. G. (2016). The dynamical generation of current sheets in astrophysical plasma turbulence. *The Astrophysical Journal Letters*, 827(2), L28. <https://doi.org/10.3847/2041-8205/827/2/L28>
- Huang, S. Y., Hadid, L. Z., Sahraoui, F., Yuan, Z. G., & Deng, X. H. (2017). On the existence of the Kolmogorov inertial range in the terrestrial magnetosheath turbulence. *The Astrophysical Journal*, 836(1), L10. <https://doi.org/10.3847/2041-8213/836/1/L10>
- Huang, S. Y., Sahraoui, F., Andrés, N., Hadid, L. Z., Yuan, Z. G., He, J. S., et al. (2021). The ion transition range of solar wind turbulence in the inner heliosphere: Parker solar probe observations. *The Astrophysical Journal Letters*, 909(1), L7. <https://doi.org/10.3847/2041-8213/abdaaf>
- Jakosky, B. M., Lin, R. P., Grebowsky, J. M., Luhmann, J. G., Mitchell, D. F., Beutelschies, G., et al. (2015). The Mars atmosphere and volatile evolution (MAVEN) mission. *Space Science Reviews*, 195(1–4), 3–48. <https://doi.org/10.1007/s11214-015-0139-x>
- Jiang, W., Li, H., Liu, X., Verscharen, D., & Wang, C. (2023). Statistical properties of Plateau-like turbulence spectra in the Martian magnetosheath: MAVEN observations. *Journal of Geophysical Research (Space Physics)*, 128(1), e2022JA030874. <https://doi.org/10.1029/2022JA030874>
- Jiang, W., Li, H., Yang, Z., Verscharen, D., & Wang, C. (2025). Spatial dependence of ion-kinetic instabilities in the Earth's magnetosheath: MMS observations. *Journal of Geophysical Research: Space Physics*, 130(3), e2024JA033463. <https://doi.org/10.1029/2024JA033463>

- Jiang, W., Verscharen, D., Jeong, S.-Y., Li, H., Klein, K. G., Owen, C. J., & Wang, C. (2024). Velocity-space signatures of resonant energy transfer between whistler waves and electrons in the Earth's magnetosheath. *The Astrophysical Journal*, 960(1), 30. <https://doi.org/10.3847/1538-4357/ad0df8>
- Jiang, W., Verscharen, D., Li, H., Wang, C., & Klein, K. G. (2022). Whistler waves as a signature of converging magnetic holes in space plasmas. *The Astrophysical Journal*, 935(2), 169. <https://doi.org/10.3847/1538-4357/ac7ce2>
- Karimabadi, H., Roytershteyn, V., Vu, H. X., Omelchenko, Y. A., Scudder, J., Daughton, W., et al. (2014). The link between shocks, turbulence, and magnetic reconnection in collisionless plasmas. *Physics of Plasmas*, 21(6), 062308. <https://doi.org/10.1063/1.4882875>
- Li, H., Jiang, W., Wang, C., Verscharen, D., Zeng, C., Russell, C. T., et al. (2020). Evolution of the Earth's magnetosheath turbulence: A statistical study based on MMS observations. *The Astrophysical Journal Letters*, 898(2), L43. <https://doi.org/10.3847/2041-8213/aba531>
- Li, H., Jiang, W., Yang, Z., Liu, X., Verscharen, D., & Wang, C. (2024). Pickup ion modulation on plateau-like turbulence in the Martian magnetosheath. *The Astrophysical Journal*, 967(2), 76. <https://doi.org/10.3847/1538-4357/ad3d49>
- Li, H., Wang, C., Richardson, J. D., & Tu, C. (2017). Evolution of Alfvénic fluctuations inside an Interplanetary coronal mass ejection and their contribution to local plasma heating: Joint observations from 1.0 to 5.4 au. *The Astrophysical Journal*, 851(1), L2. <https://doi.org/10.3847/2041-8213/aa9c3f>
- Lion, S., Alexandrova, O., & Zaslavsky, A. (2016). Coherent events and spectral shape at ion kinetic scales in the fast solar wind turbulence. *The Astrophysical Journal*, 824(1), 47. <https://doi.org/10.3847/0004-637X/824/1/47>
- Lucek, E. A., Horbury, T. S., Dandouras, I., & Rème, H. (2008). Cluster observations of the Earth's quasi-parallel bow shock: Cluster at the parallel bow shock. *Journal of Geophysical Research*, 113(A7). <https://doi.org/10.1029/2007JA012756>
- Marino, R., & Sorriso-Valvo, L. (2023). Scaling laws for the energy transfer in space plasma turbulence. *Physics Reports*, 1006, 1–144. <https://doi.org/10.1016/j.physrep.2022.12.001>
- Matsunaga, K., Seki, K., Brain, D. A., Hara, T., Masunaga, K., Mcfadden, J. P., et al. (2017). Statistical study of relations between the induced magnetosphere, ion composition, and pressure balance boundaries around Mars based on MAVEN observations: The Martian plasma boundaries. *Journal of Geophysical Research: Space Physics*, 122(9), 9723–9737. <https://doi.org/10.1002/2017JA024217>
- McFadden, J. P., Kortmann, O., Curtis, D., Dalton, G., Johnson, G., Abiad, R., et al. (2015). MAVEN SupraThermal and thermal ion composition (STATIC) instrument. *Space Science Reviews*, 195(1–4), 199–256. <https://doi.org/10.1007/s11214-015-0175-6>
- Osman, K. T., Matthaeus, W. H., Greco, A., & Servidio, S. (2011). Evidence for inhomogeneous heating in the solar wind. *The Astrophysical Journal Letters*, 727(1), L11. <https://doi.org/10.1088/2041-8205/727/1/L11>
- Pitňa, A., Šafránková, J., Němeček, Z., Goncharov, O., Němec, F., Přech, L., et al. (2016). Density fluctuations upstream and downstream of interplanetary shocks. *The Astrophysical Journal*, 819(1), 41. <https://doi.org/10.3847/0004-637X/819/1/41>
- Pitňa, A., Šafránková, J., Němeček, Z., Pi, G., Zank, G., Zhao, L., et al. (2024). Turbulent heating of solar wind plasma downstream of magnetohydrodynamic shocks. *The Astrophysical Journal*, 963(2), 161. <https://doi.org/10.3847/1538-4357/ad1c64>
- Politano, H., & Pouquet, A. (1998). von Kármán–Howarth equation for magnetohydrodynamics and its consequences on third-order longitudinal structure and correlation functions. *Physical Review*, 57(1), R21–R24. <https://doi.org/10.1103/PhysRevE.57.R21>
- Rahmati, A., Larson, D. E., Cravens, T. E., Lillis, R. J., Halekas, J. S., McFadden, J. P., et al. (2017). MAVEN measured oxygen and hydrogen pickup ions: Probing the Martian exosphere and neutral escape. *Journal of Geophysical Research: Space Physics*, 122(3), 3689–3706. <https://doi.org/10.1002/2016JA023371>
- Rakhmanova, L., Riazantseva, M., Zastenker, G., & Verigin, M. (2018). Kinetic-scale ion flux fluctuations behind the quasi-parallel and quasi-perpendicular bow shock. *Journal of Geophysical Research: Space Physics*, 123(7), 5300–5314. <https://doi.org/10.1029/2018JA025179>
- Rakhmanova, L., Riazantseva, M., Zastenker, G., Yermolaev, Y., & Lodkina, I. (2020). Dynamics of plasma turbulence at earth's bow shock and through the magnetosheath. *The Astrophysical Journal*, 901(1), 30. <https://doi.org/10.3847/1538-4357/abae00>
- Romanelli, N., Andrés, N., & DiBraccio, G. A. (2022). Variability of the incompressible energy Cascade rate in solar wind turbulence around Mars. *The Astrophysical Journal*, 929(2), 145. <https://doi.org/10.3847/1538-4357/ac5902>
- Romanelli, N., Bertucci, C., Gómez, D., Mazelle, C., & Delva, M. (2013). Proton cyclotron waves upstream from Mars: Observations from Mars global surveyor. *Planetary and Space Science*, 76, 1–9. <https://doi.org/10.1016/j.pss.2012.10.011>
- Romanelli, N., Mazelle, C., Chaufray, J. Y., Meziane, K., Shan, L., Ruhunusiri, S., et al. (2016). Proton cyclotron waves occurrence rate upstream from Mars observed by MAVEN: Associated variability of the Martian upper atmosphere: Temporal variability of PCWs. *Journal of Geophysical Research: Space Physics*, 121(11), 11113–11128. <https://doi.org/10.1002/2016JA023270>
- Ruhunusiri, S., Halekas, J. S., Espley, J. R., Mazelle, C., Brain, D., Harada, Y., et al. (2017). Characterization of turbulence in the Mars plasma environment with MAVEN observations. *Journal of Geophysical Research: Space Physics*, 122(1), 656–674. <https://doi.org/10.1002/2016JA023456>
- Sahraoui, F., Belmont, G., Rezeau, L., Cornilleau-Wehrlin, N., Pinçon, J. L., & Balogh, A. (2006). Anisotropic turbulent spectra in the terrestrial magnetosheath as seen by the cluster spacecraft. *Physical Review Letters*, 96(7), 075002. <https://doi.org/10.1103/PhysRevLett.96.075002>
- Sahraoui, F., Hadid, L., & Huang, S. (2020). Magnetohydrodynamic and kinetic scale turbulence in the near-Earth space plasmas: A (short) biased review. *Reviews of Modern Plasma Physics*, 4(1), 4. <https://doi.org/10.1007/s41614-020-0040-2>
- Sanchez-Cano, B., Opgenoorth, H., Leblanc, F., Andrews, D., & Lester, M. (2022). The M-MATISSE mission: Mars magnetosphere ATMosphere ionosphere and surface Science. *44th cospar scientific assembly* (Vol. 44, p. 421). held 16-24 july.
- Schwartz, S. J., & Burgess, D. (1991). Quasi-parallel shocks: A patchwork of three-dimensional structures. *Geophysical Research Letters*, 18(3), 373–376. <https://doi.org/10.1029/91GL00138>
- Simon, P., & Sahraoui, F. (2022). Exact law for compressible pressure-anisotropic magnetohydrodynamic turbulence: Toward linking energy Cascade and instabilities. *Physical Review E—Statistical Physics, Plasmas, Fluids, and Related Interdisciplinary Topics*, 105(5), 055111. <https://doi.org/10.1103/PhysRevE.105.055111>
- Sioulas, N., Velli, M., Huang, Z., Shi, C., Bowen, T. A., Chandran, B. D. G., et al. (2023). On the evolution of the anisotropic scaling of magnetohydrodynamic turbulence in the inner heliosphere. *The Astrophysical Journal*, 951(2), 141. <https://doi.org/10.3847/1538-4357/acc658>
- Sorriso-Valvo, L., Yordanova, E., Dimmock, A. P., & Telloni, D. (2021). Turbulent cascade and energy transfer rate in a solar coronal mass ejection. *The Astrophysical Journal Letters*, 919(2), L30. <https://doi.org/10.3847/2041-8213/ac26c5>
- Soucek, J., Escoubet, C. P., & Grison, B. (2015). Magnetosheath plasma stability and ULF wave occurrence as a function of location in the magnetosheath and upstream bow shock parameters. *Journal of Geophysical Research: Space Physics*, 120(4), 2838–2850. <https://doi.org/10.1002/2015JA021087>
- Taylor, G. I. (1937). The spectrum of turbulence. *Proceedings of the royal society of London. Series A-mathematical and physical sciences* (Vol. 164(919), pp. 476–490). <https://doi.org/10.1098/rspa.1938.0032>
- Terres, M., & Li, G. (2021). Relating the solar wind turbulence spectral break at the dissipation range with an upstream spectral bump at planetary bow shocks. *arXiv:2108.07048*. [physics].

- Trotignon, J., Mazelle, C., Bertucci, C., & Acuña, M. (2006). Martian shock and magnetic pile-up boundary positions and shapes determined from the Phobos 2 and Mars global surveyor data sets. *Planetary and Space Science*, 54(4), 357–369. <https://doi.org/10.1016/j.pss.2006.01.003>
- Tu, C. Y., & Marsch, E. (1995). MHD structures, waves and turbulence in the solar wind: Observations and theories. *Space Science Reviews*, 73(1–2), 1–210. <https://doi.org/10.1007/BF00748891>
- Turc, L., Roberts, O. W., Verscharen, D., Dimmock, A. P., Kajdič, P., Palmroth, M., et al. (2023). Transmission of foreshock waves through Earth's bow shock. *Nature Physics*, 19(1), 78–86. <https://doi.org/10.1038/s41567-022-01837-z>
- Verscharen, D., Klein, K. G., & Maruca, B. A. (2019). The multi-scale nature of the solar wind. *Living Reviews in Solar Physics*, 16(1), 5. <https://doi.org/10.1007/s41116-019-0021-0>
- Vörös, Z., Zhang, T. L., Leaner, M. P., Volwerk, M., Delva, M., & Baumjohann, W. (2008). Intermittent turbulence, noisy fluctuations, and wavy structures in the Venusian magnetosheath and wake. *Journal of Geophysical Research (Planets)*, 113(E12), E00B21. <https://doi.org/10.1029/2008JE003159>
- Yordanova, E., Vaivads, A., André, M., Buchert, S. C., & Vörös, Z. (2008). Magnetosheath plasma turbulence and its spatiotemporal evolution as observed by the cluster spacecraft. *Physical Review Letters*, 100(20), 205003. <https://doi.org/10.1103/PhysRevLett.100.205003>
- Zank, G. P., Nakanotani, M., Zhao, L. L., Du, S., Adhikari, L., Che, H., & Le Roux, J. A. (2021). Flux ropes, turbulence, and collisionless perpendicular shock waves: High plasma beta case. *The Astrophysical Journal*, 913(2), 127. <https://doi.org/10.3847/1538-4357/abf7c8>
- Zank, G. P., Zhao, L.-L., Adhikari, L., Nakanotani, M., Pitňa, A., Telloni, D., & Che, H. (2023). Linear mode decomposition in magnetohydrodynamics revisited. *The Astrophysical Journal—Supplement Series*, 268(1), 18. <https://doi.org/10.3847/1538-4365/acdf5d>

References From the Supporting Information

- Boldyrev, S., Carlos Perez, J., Borovsky, J. E., & Podesta, J. J. (2011). Spectral scaling laws in magnetohydrodynamic turbulence simulations and in the solar wind. *The Astrophysical Journal*, 741(1), L19. <https://doi.org/10.1088/2041-8205/741/1/L19>
- Chen, C. H. K., Bale, S. D., Bonnell, J. W., Borovikov, D., Bowen, T. A., Burgess, D., et al. (2020). The evolution and role of solar wind turbulence in the inner heliosphere. *The Astrophysical Journal—Supplement Series*, 246(2), 53. <https://doi.org/10.3847/1538-4365/ab60a3>